Journal of Innovative Optical Health Sciences
Vol. 3, No. 4 (2010) 267–277
© World Scientific Publishing Company
DOI: 10.1142/S179354581000112X

World Scientific
www.worldscientific.com

J. Innov. Opt. Health Sci. 2010.03:267-277. Downloaded from www.worldscientific.com
by HUAZHONG UNIVERSITY OF SCIENCE AND TECHNOLOGY on 10/24/18. Re-use and distribution is strictly not permitted, except for Open Access articles.

NEAR-INFRARED, BROAD-BAND SPECTRAL IMAGING OF THE HUMAN BREAST FOR QUANTITATIVE OXIMETRY: APPLICATIONS TO HEALTHY AND CANCEROUS BREASTS

YANG YU[*,§], ANGELO SASSAROLI[*], DEBBIE K. CHEN[*],
MARC J. HOMER[†], ROGER A. GRAHAM[‡] and SERGIO FANTINI[*]
[*]*Department of Biomedical Engineering, Tufts University*
4 Colby Street, Medford, MA 02155, USA
[†]*Tufts Medical Center, Department of Radiology*
800 Washington Street, Boston, MA 02111, USA
[‡]*Tufts Medical Center, Department of Surgery*
800 Washington Street, Boston, MA 02111, USA
[§]*yang.yu@tufts.edu*

We have examined ten human subjects with a previously developed instrument for near-infrared diffuse spectral imaging of the female breast. The instrument is based on a tandem, planar scan of two collinear optical fibers (one for illumination and one for collection) to image a gently compressed breast in a transmission geometry. The optical data collection features a spatial sampling of 25 points/cm^2 over the whole breast, and a spectral sampling of 2 points/nm in the 650–900 nm wavelength range. Of the ten human subjects examined, eight are healthy subjects and two are cancer patients with unilateral invasive ductal carcinoma and ductal carcinoma *in situ*, respectively. For each subject, we generate second-derivative images that identify a network of highly absorbing structures in the breast that we assign to blood vessels. A previously developed paired-wavelength spectral method assigns oxygenation values to the absorbing structures displayed in the second-derivative images. The resulting oxygenation images feature average values over the whole breast that are significantly lower in cancerous breasts ($69 \pm 14\%$, $n = 2$) than in healthy breasts ($85 \pm 7\%$, $n = 18$) ($p < 0.01$). Furthermore, in the two patients with breast cancer, the average oxygenation values in the cancerous regions are also significantly lower than in the remainder of the breast (invasive ductal carcinoma: $49 \pm 11\%$ vs $61 \pm 16\%$, $p < 0.01$; ductal carcinoma *in situ*: $58 \pm 8\%$ vs $77 \pm 11\%$, $p < 0.001$).

Keywords: Diffuse spectral imaging; near-infrared spectroscopy; optical mammography; oximetry; hemoglobin saturation.

1. Introduction

Diffuse optical imaging methods[1] for breast cancer detection and monitoring have developed into a mature technology that is ready for pilot clinical trials and studies on populations of healthy and diseased breasts.[2] While most breast lesions feature a significant intrinsic optical contrast that allows for their detection with optical mammography, the major challenge faced by this technology is the discrimination of normal lesions, benign tumors, and cancer. One option to address this challenge is to go beyond a self-contained, intrinsic-contrast-based

J. Innov. Opt. Health Sci. 2010.03:267-277. Downloaded from www.worldscientific.com
by HUAZHONG UNIVERSITY OF SCIENCE AND TECHNOLOGY on 10/24/18. Re-use and distribution is strictly not permitted, except for Open Access articles.

optical mammography method. For example, a number of studies have explored the introduction of extrinsic fluorescent contract agents,[3,4] or the synergistic combination of optical mammography with established medical imaging techniques such as X-ray imaging,[5] magnetic resonance imaging,[6] or ultrasound imaging.[7] While introducing extrinsic contrast agents and performing complementary examinations with adjunct imaging modalities can significantly enrich the information content of the data collected, these approaches also compromise appealing features of optical mammography such as non-invasiveness, repeatability of application, and relatively compact instrumentation. A second option to tackle the problem of discrimination of benign and cancerous breast lesions is to apply optical mammography as a stand-alone technique where the information content of its data is enriched either by collecting a more complete dataset or by introducing data processing methods capable of extracting additional information from a given dataset. A number of studies have explored this option, for example by extending the spectral range of optical mammography to 1,000 nm for sensitivity to lipids and water[8–10] and to 1,060 nm for sensitivity to collagen,[11] by developing quantitative three-dimensional optical tomography approaches,[12] by introducing computer-aided detection methods based on diffuse optical tomography images,[13] or by collecting dynamic optical images of the breast in response to a physiological challenge[14] or mechanical compression.[15]

In this work, we explore the potential of optical mammography to develop into a stand-alone clinical modality by considering two key facts, namely (1) the extremely high intrinsic optical contrast provided by blood (which is two orders of magnitudes more absorbing than breast tissue in the near infrared), and (2) the strong spectral dependence of blood absorption on the oxygen saturation of hemoglobin. These two facts account for the high sensitivity of optical mammography to blood vessels (or tissue regions of elevated vascular density) and to their oxygenation level. Even though reports of breast cancer oxygenation as measured with near-infrared spectroscopy have not consistently found it to be a robust parameter for discrimination of benign and malignant lesions, it is nevertheless reasonable to expect oxygen saturation of hemoglobin to be reduced at cancerous sites as a result of the increased metabolic demand of cancer and the impaired blood flow in the tortuous and abnormal angiogenic vasculature. This is why, in this work, we place emphasis on the application of a new paired-wavelength spectral approach to tumor oximetry,[16] based on a second-derivative enhancement of the spatial distribution of a network of highly absorbing regions within breast tissue.[17] We report and discuss the results obtained from ten human subjects, of which two are affected by breast cancer, where we typically observe lower oxygenation values associated with cancerous breasts (versus healthy breasts) and with cancerous tissue regions (versus the remainder of the same breast).

2. Methods

2.1. *Instrument for spectral imaging of the breast*

The block diagram of the instrument for spectral imaging of the breast, previously reported in Ref. 18, is shown in Fig. 1. The light source is an arc lamp (Model No. 6258, Oriel Instrument, Stratford, CT) whose emission is first spectrally filtered (400–1,000 nm) to reject ultraviolet and infrared light, and then focused onto a 3-mm-diameter illumination optical glass fiber bundle (NA: 0.56), which delivers light to the breast with an average illumination power of 325 mW, which translates into a power density of $4.6\,\mathrm{W/cm^2}$. A 5-mm-diameter collection optical glass fiber bundle (NA: 0.66) is located on the opposite side of the breast, and always kept collinear with the illumination optical fiber. The breast is gently compressed to stabilize the position of the breast while the scan is being performed, without causing any discomfort to the subject, between two parallel glass plates whose distance is recorded for every examination. The collection optical fiber delivers light to a spectrograph (Model No. SP-150, Acton Research Corp., Acton, MA), which disperses the light onto the detector array of a charge coupled device (CCD) camera (Model No. DU420A-BR-DD, Andor Technology, South Windsor, CT). The CCD camera exposure time of 45 ms and the readout time of 12 ms result in a sampling rate of $1/(57\,\mathrm{ms}) = 17.5\,\mathrm{Hz}$ for the collection of full spectral data. The spectrograph features a grating blazed at 700 nm with 350 g/mm, resulting in a dispersion of 20 nm/mm at the exit port. The size of the CCD camera pixels of $26\,\mu\mathrm{m} \times 26\,\mu\mathrm{m}$ results in a spectral sampling rate of two data points per nanometer, even though the spectral resolution is not as high because of the size

J. Innov. Opt. Health Sci. 2010.03:267-277. Downloaded from www.worldscientific.com
by HUAZHONG UNIVERSITY OF SCIENCE AND TECHNOLOGY on 10/24/18. Re-use and distribution is strictly not permitted, except for Open Access articles.

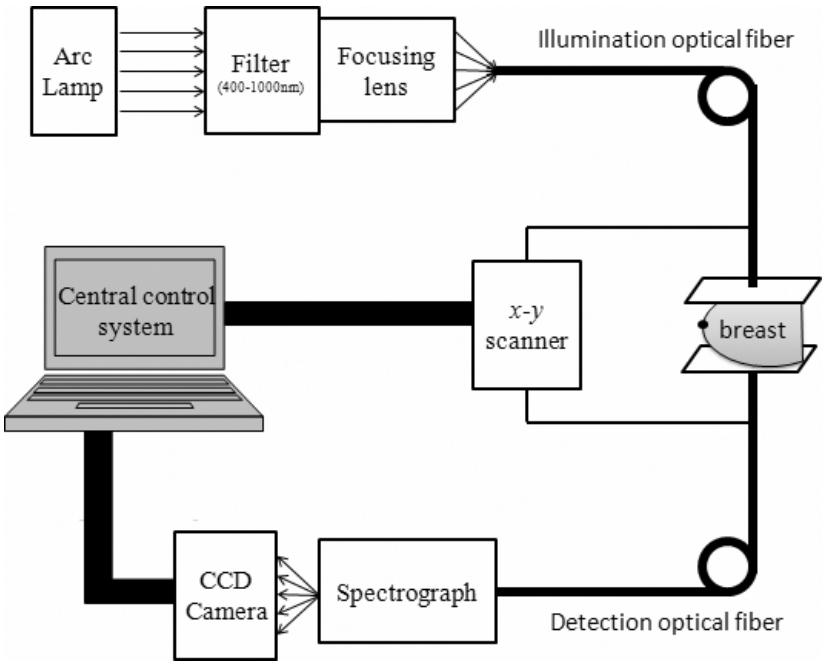

Fig. 1. Block diagram of the instrument for spectral imaging of the human breast. CCD: charge coupled device. Breast tissue, gently compressed between two glass plates, is being probed by a single source–detector pair in a transmission geometry. Spectral information is acquired through a combination of spectrograph/CCD system, whose photon count is used as the real-time feedback signal to trigger the scanner to the next scanning line when the detected photon number is above the threshold. A raw breast image and the most recent spectrum are being displayed on the computer screen concurrently while the scan is being performed, allowing a rough estimate of the region of interest and associated signal-to-noise ratio.

of the entrance slit (2 mm) used to accommodate the large collection optical fiber bundle. However, spectral resolution is not critical in this application, where all chromophores of interest in breast tissue (oxy-hemoglobin, deoxy-hemoglobin, water, lipids) feature broad absorption spectral bands. Of the full measured spectral range, we only retain the wavelength band 650–900 nm over which the signal-to-noise ratio is adequate. The illumination and collection optical fibers are scanned in tandem, line by line, over the $x-y$ plane defined by the glass plates used to keep the breast in a stable position. Scanning is limited to the region occupied by the breast by a feedback system that switches to the next scanning line once the optical transmission through the breast exceeds a given threshold, which indicates that the breast edge has been reached. The scanning speed along the scanning direction (x) is 3.5 cm/s. In combination with the spectral acquisition rate of 17.5 Hz, it results in the collection of one optical data point every 2 mm along x. Each line (x) is scanned twice, first along $+x$ and then along $-x$. The purpose of this double scan is a more accurate spatial assignment of the acquired spectra, by correcting for the slight offset between rightward and leftward scanning lines introduced by the finite time needed by the stepper motors to come to a stop at the end of each line. By scanning the same line twice in opposite directions and taking the average of the data collected in each position during the two scans, we minimize the effect of the slight directional offset. Successive scanning lines are separated by 2 mm in the y-direction so that optical data are collected every 2 mm along y as well, and the instrument therefore collects 25 full optical spectra per square centimeter of the examined breast.

A handheld optical probe featuring multiple source-detector separations and connected to a separate, frequency-domain tissue spectrometer (OxiplexTS, ISS Inc., Champaign, IL) is used to measure the reduced scattering coefficients of bulk breast tissue at two wavelengths (690 and 830 nm). Measurements are conducted at two to three different locations of each breast from which we obtain an average value for μ_s' at two wavelengths that are then extrapolated to a full scattering spectrum as required by the application of the paired-wavelength spectral oximetry approach employed by us.[16]

J. Innov. Opt. Health Sci. 2010.03:267-277. Downloaded from www.worldscientific.com
by HUAZHONG UNIVERSITY OF SCIENCE AND TECHNOLOGY on 10/24/18. Re-use and distribution is strictly not permitted, except for Open Access articles.

2.2. *Data processing*

The original data set from the CCD camera consists of a string of N spectra (each consisting of ∼500 spectral data points), one spectrum per image pixel (the total number N of acquired pixels per image ranges from a minimum of ∼1,000 to a maximum of ∼2,700 in the cases reported in this work). This string of N spectra is rearranged into a 2D spatial distribution corresponding to the $x-y$ scanning plane by proper synchronization of the CCD data collection with the mechanical scanning of the optical fibers. In this way, we obtain spectral optical maps representing a 2D projection image of the breast. On these spectral optical maps, we perform a 2D cubic spline interpolation in the x–y plane to generate smoother images that are the starting point for the image processing steps described below.

Two-dimensional projection images generated by a planar scan of the breast suffer from so-called edge effects, resulting from the tissue thickness variability over the imaged area and particularly in the vicinity of the breast edge. In the past, we have used frequency-domain data to correct for edge effects.[19] In this work, we have performed a correction for edge effects using solely continuous wave data, by noting that the spatial frequencies associated with edge effects are typically lower than those associated with breast inhomogeneities, blood vessels, and breast lesions. Therefore, we have applied a low-pass spatial filter (cutoff frequency: $1.8\,\mathrm{cm}^{-1}$) to the data and then taken a ratio between the original data and the low-pass filtered data to suppress edge effects while retaining higher spatial frequency components.

On the edge corrected images, we have applied a second low-pass spatial frequency filter (a binomial filter using data over an area of $1\,\mathrm{cm}^2$ around each pixel, thus featuring a cutoff frequency of $0.64\,\mathrm{cm}^{-1}$) to suppress high-frequency noise in the images. Finally, a spatial second-derivative algorithm, which assigns to each pixel the minimum value of the second derivative along four directions $(\mathbf{x}, \mathbf{y}, \mathbf{x}+\mathbf{y}, \mathbf{x}-\mathbf{y})$, is applied to enhance the detection of regions of locally increased absorption in the breast.[17] Second-derivative images display, on a gray scale, only negative second-derivative values, so that these images identify regions of localized higher absorption in the breast.

We have applied a paired-wavelength spectral method[16] to assign an oxygenation value to the image pixels that feature a local maximum in absorption as identified by the second-derivative images. Such oxygenation value refers to the oxygen saturation of hemoglobin in breast tissue, and it is therefore indicated as StO_2. We have generated oxygenation images displaying the oxygenation values on a color scale, and built histograms of oxygenation values for all pixels to which the paired-wavelength spectral oximetry approach was applied.

2.3. *Human subjects and imaging protocol*

We have investigated ten human subjects. Eight of them are healthy volunteers, age range 19–35 years, while two of them (subject Nos. 16 and 17, ages 68 and 56 years, respectively) are breast cancer patients recruited at the Tufts Medical Center, Boston, MA. X-ray mammography, performed before the optical mammograms, and fine needle biopsy, performed after the optical mammograms, found an invasive ductal carcinoma in the right breast of subject No. 16, and a ductal carcinoma *in situ* in the right breast of subject No. 17. All subjects were examined in a dedicated room, first with a handheld optical probe for frequency-domain measurements of the average reduced scattering coefficient of breast tissue, and then with the spectral imaging system for optical mammography. The breasts were imaged in craniocaudal (cc) view. The time required to image each breast ranged from three to six minutes, depending on breast size, and the total measurement procedure (preliminary frequency-domain scattering measurements + imaging of both breasts) typically took about 15 to 20 minutes.

3. Results

In all ten subjects investigated, we have consistently observed second-derivative breast images that feature a network of highly absorbing structures that we assign to blood vessels or to tissue regions with higher vascular density. The oxygenation values associated with these highly absorbing structures make up the oxygenation images and are also displayed in histograms to better visualize their statistical distribution. These are the results that we report in this section, namely second-derivative images, oxygenation images, and histograms of the distribution of oxygenation values.

Table 1 lists the age, ethnicity/race, the separation between the glass plates in each breast

J. Innov. Opt. Health Sci. 2010.03:267-277. Downloaded from www.worldscientific.com
by HUAZHONG UNIVERSITY OF SCIENCE AND TECHNOLOGY on 10/24/18. Re-use and distribution is strictly not permitted, except for Open Access articles.

Table 1. Summary of the results of breast oxygenation mapping on the ten subjects. Ethnicity (Ethn) is either Hispanic (H) or not Hispanic (NH). Race is African American (AA), or White (Wh). The glass plate separation corresponds to the maximum thickness of the imaged breast tissue. L: left breast; R: right breast. The stars next to subject Nos. 16 and 17 indicate that these are the two breast cancer patients, both with cancer in their right breast. The StO_2 column reports the average and standard deviation of the distribution of oxygenation values in the image, as illustrated in the oxygenation histograms.

Subject No.	Age (y)	Ethn/race	Side	Plate separ. (cm)	StO_2 (%) ave +/− std	Oxygenation histogram
9	25	NH/Wh	L	6.0	88 ± 9	
			R	5.5	91 ± 5	
10	24	NH/Wh	L	7.2	83 ± 7	
			R	7.2	87 ± 7	
11	22	NH/AA	L	5.0	87 ± 11	
			R	5.0	86 ± 10	
12	20	NH/Wh	L	5.0	87 ± 7	
			R	5.0	83 ± 5	
13	35	NH/Wh	L	6.0	87 ± 6	
			R	6.0	86 ± 7	
14	19	NH/Wh	L	6.0	83 ± 8	
			R	6.0	88 ± 5	
15	25	NH/Wh	L	5.5	92 ± 2	
			R	5.5	90 ± 2	
16*	68	H/Wh	L	4.5	60 ± 14	
			R*	4.5	61 ± 17	
17*	56	NH/Wh	L	6.5	83 ± 5	
			R*	6.4	77 ± 12	
18	20	NH/Wh	L	5.5	83 ± 4	
			R	5.5	82 ± 4	

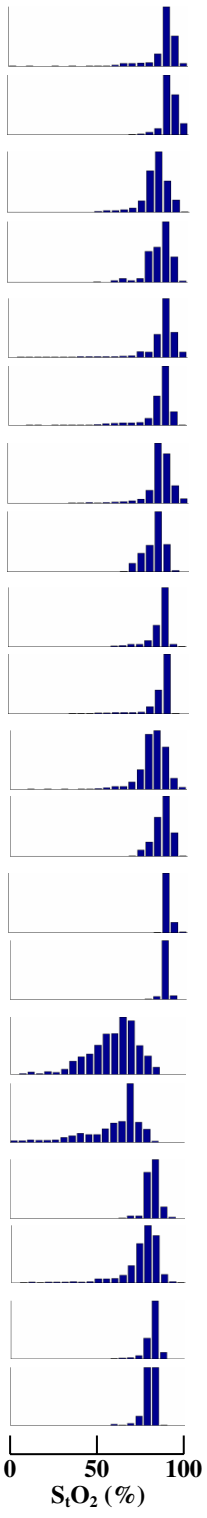

J. Innov. Opt. Health Sci. 2010.03:267-277. Downloaded from www.worldscientific.com
by HUAZHONG UNIVERSITY OF SCIENCE AND TECHNOLOGY on 10/24/18. Re-use and distribution is strictly not permitted, except for Open Access articles.

examination, the average ± standard deviation of the distribution of oxygenation values (StO_2) over the imaged breast, and the histogram of the StO_2 distribution for all subjects. The two breast cancer patients (subject Nos. 16 and 17) and their diseased breasts (right) are identified by a star (*) in Table 1.

3.1. *Healthy subjects*

Figure 2 shows the optical mammograms of both breasts of subject No. 11, a healthy 22-year-old African American. The high melanin content in the skin does not hinder optical mammography because it is confined to a thin superficial layer and is not dramatically reducing light transmission into and out of the breast. The average reduced scattering coefficients measured at two wavelengths with frequency-domain spectroscopy were μ_s' (690 nm) = 9.4 cm^{-1} and μ_s' (830 nm) = 8.4 cm^{-1} for her right breast, and μ_s' (690 nm) = 7.2 cm^{-1} and μ_s' (830 nm) = 6.3 cm^{-1} for her left breast. The second-derivative images [Fig. 2, panels (a) and (b)] identify regions of higher absorption to which oxygenation values are assigned to generate oxygenation images [Fig. 2, panels (c) and (d)]. The histograms of the distribution of oxygenation values [Fig. 2, panels (e) and (f)] show averages (± standard deviations) of 87 ± 11% (left breast) and 86 ± 10% (right breast). These are relatively narrow distributions around

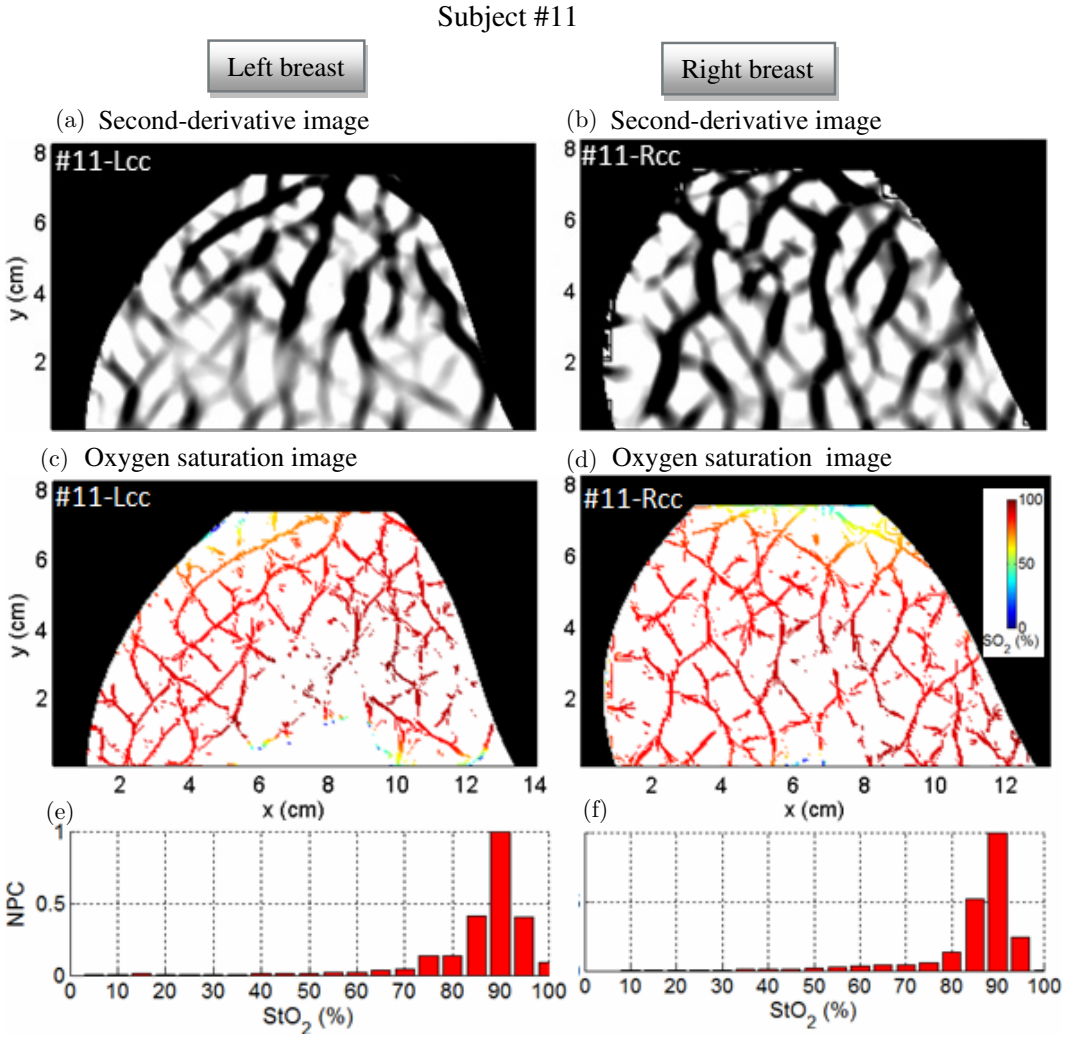

Fig. 2. Optical mammograms in a craniocaudal (cc) projection and oxygenation histograms for subject No. 11, a healthy 22-year-old African American volunteer. Panels (a) and (b) are second-derivative images, panels (c) and (d) are oxygenation images, and panels (e) and (f) are oxygenation histograms reporting the normalized pixel counts (NPC) corresponding to oxygenation values over the entire 0–100% range. Left panels [(a), (c) and (e)] refer to the left breast. Right panels [(b), (d) and (f)] refer to the right breast. The average oxygenation values in (c) and (d), as computed from the corresponding histograms in (e) and (f), are 87% for the left breast and 86% for the right breast.

J. Innov. Opt. Health Sci. 2010.03:267-277. Downloaded from www.worldscientific.com
by HUAZHONG UNIVERSITY OF SCIENCE AND TECHNOLOGY on 10/24/18. Re-use and distribution is strictly not permitted, except for Open Access articles.

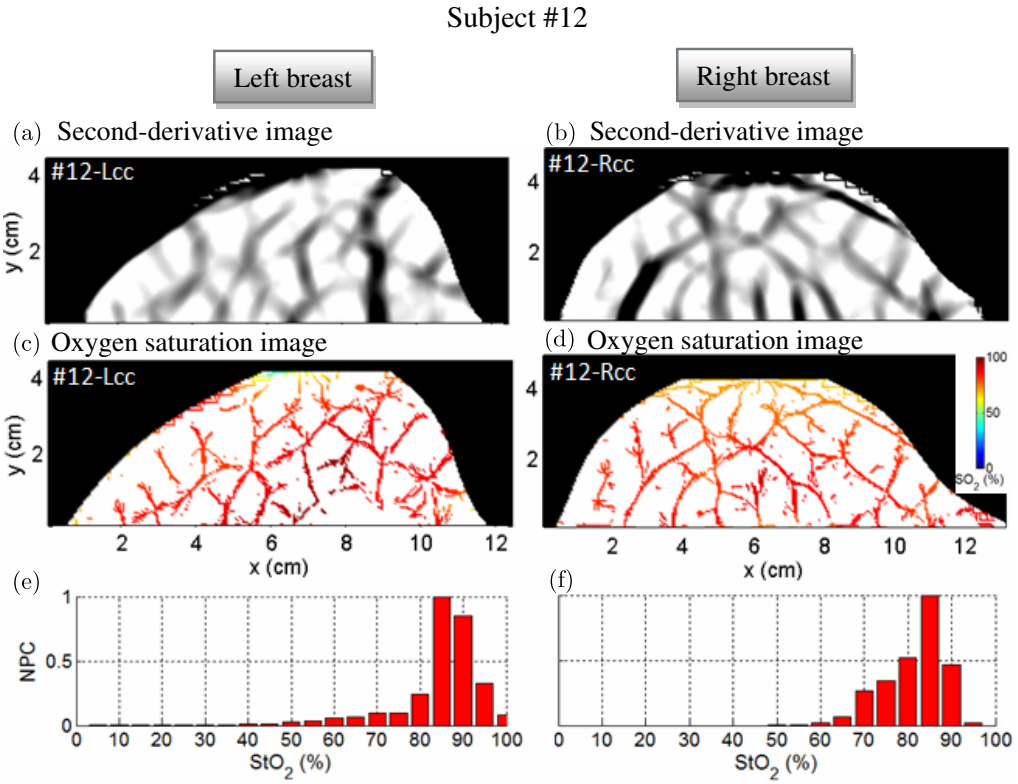

Fig. 3. Optical mammograms in a craniocaudal (cc) projection and oxygenation histograms for subject No. 12, a healthy 20-year-old Caucasian volunteer. Panels (a) and (b) are second-derivative images, panels (c) and (d) are oxygenation images, and panels (e) and (f) are oxygenation histograms reporting the normalized pixel counts (NPC) corresponding to oxygenation values over the entire 0–100% range. Left panels [(a), (c) and (e)] refer to the left breast. Right panels [(b), (d) and (f)] refer to the right breast. The average oxygenation values in (c) and (d), as computed from the corresponding histograms in (e) and (f), are 87% for the left breast and 83% for the right breast.

high oxygen saturation values throughout breast tissue.

Figure 3 shows the results for subject No. 12, a healthy 20-year-old Caucasian female. The average reduced scattering coefficients were μ_s' (690 nm) = 8.2 cm^{-1} and μ_s' (830 nm) = 7.6 cm^{-1} for her right breast, and μ_s' (690 nm) = 7.6 cm^{-1} and μ_s' (830 nm) = 6.5 cm^{-1} for her left breast. The histograms of the distribution of oxygenation values [Fig. 3, panels (e) and (f)] show averages ($\pm$ standard deviations) of $87 \pm 7\%$ (left breast) and $83 \pm 5\%$ (right breast). Similarly to the case of subject No. 11, these values indicate relatively narrow distributions around high oxygen saturation values throughout breast tissue.

3.2. *Cancer patients*

Figure 4 shows the results for subject No. 16, a 68-year-old Hispanic female with an invasive ductal carcinoma (IDC) in her right breast. The average reduced scattering coefficients were μ_s' (690 nm) = 7.0 cm^{-1} and μ_s' (830 nm) = 6.6 cm^{-1} for her right breast, and μ_s' (690 nm) = 4.7 cm^{-1} and μ_s' (830 nm) = 4.5 cm^{-1} for her left breast. The oxygenation values measured with spectral optical imaging at the cancerous area (as identified by X-ray mammography), highlighted in Fig. 4(d), indicate a hypoxic state. In fact, the distribution of oxygenation values at the cancerous site [blue histogram in Fig. 4(f)], indicates a significantly lower average oxygenation around cancerous tissue ($49 \pm 11\%$) than in the remainder of the breast ($61 \pm 16\%$) ($p < 0.01$). However, a more strongly hypoxic area at around $x \sim 9$ cm, $y \sim 1$ cm was observed at a distance of about 2 cm from the cancer location. Furthermore, the average oxygenation values in both breasts (left: $60 \pm 14\%$; right: $61 \pm 17\%$) was significantly lower than those in the healthy subjects.

Figure 5 shows the results for subject No. 17, a 56-year-old Caucasian female with ductal carcinoma *in situ* (DCIS) in her right breast. The average reduced scattering coefficients were μ_s'

J. Innov. Opt. Health Sci. 2010.03:267-277. Downloaded from www.worldscientific.com
by HUAZHONG UNIVERSITY OF SCIENCE AND TECHNOLOGY on 10/24/18. Re-use and distribution is strictly not permitted, except for Open Access articles.

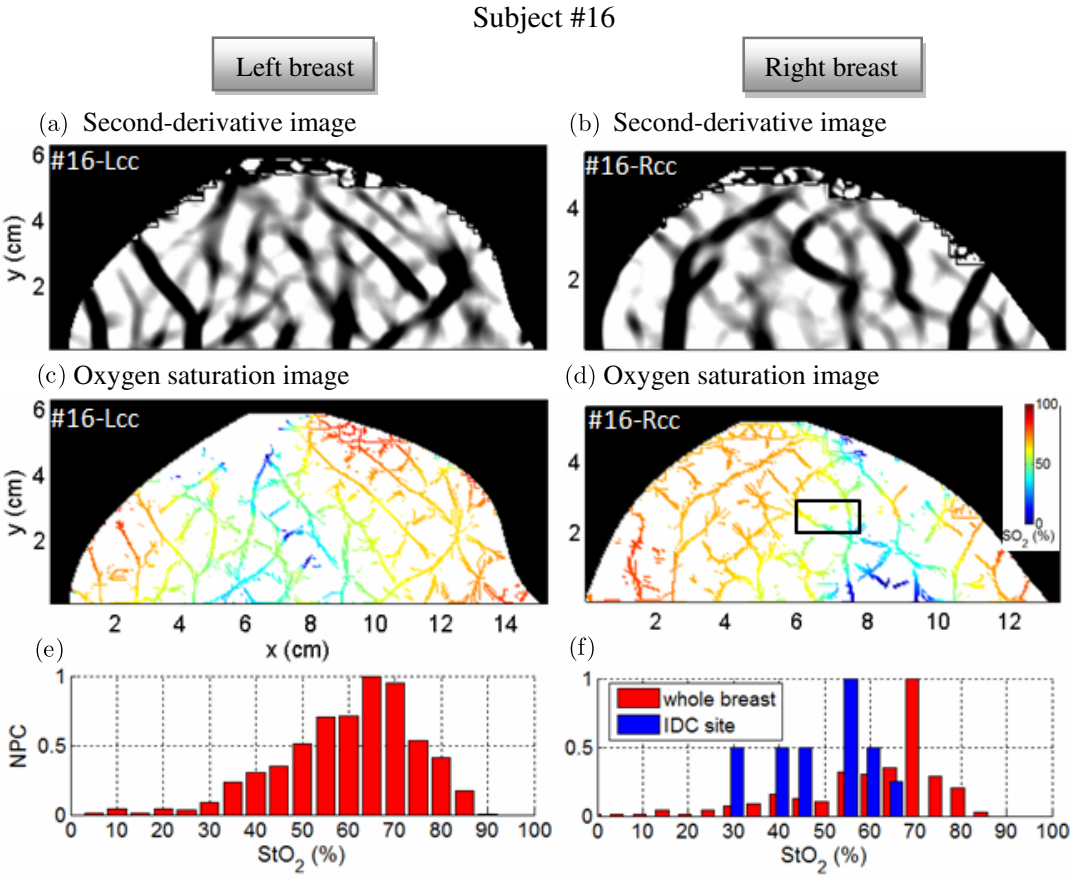

Fig. 4. Optical mammograms in a craniocaudal (cc) projection and oxygenation histograms for subject No. 16, a 68-year-old Hispanic patient with an invasive ductal carcinoma (IDC) in her right breast. Panels (a) and (b) are second-derivative images, panels (c) and (d) are oxygenation images, and panels (e) and (f) are oxygenation histograms reporting the normalized pixel counts (NPC) corresponding to oxygenation values over the entire 0–100% range. Left panels [(a), (c) and (e)] refer to the left breast. Right panels [(b), (d) and (f)] refer to the right breast. The average oxygenation values in (c) and (d), as computed from the corresponding histograms in (e) and (f), are 60% for the left breast and 61% for the right breast. The histogram of the distribution of oxygenation values within the cancer region highlighted in panel (d) is shown by the blue bars in panel (f), which feature an average oxygenation of 49%.

(690 nm) = 5.2 cm^{-1} and μ_s' (830 nm) = 4.8 cm^{-1} for her right breast, and μ_s' (690 nm) = 5.7 cm^{-1} and μ_s' (830 nm) = 5.3 cm^{-1} for her left breast. Similarly to the case of subject No. 16, the oxygenation values measured with spectral optical imaging at the cancerous area (as identified by X-ray mammography), highlighted in Fig. 5(d), indicate a hypoxic state. In fact, the distribution of oxygenation values at the cancerous site [blue histogram in Fig. 5(f)], indicates a significantly lower average oxygenation around cancerous tissue ($58 \pm 8\%$) than in the remainder of the breast ($77 \pm 11\%$) ($p < 0.001$). The average oxygenation values in the cancerous breasts (right: $77 \pm 12\%$) were significantly lower than those in healthy subjects, while those in the healthy breast (left: $83 \pm 5\%$) were comparable to those in healthy subjects.

4. Discussion

The second-derivative optical mammograms [panels (a) and (b) of Figs. 2–5] display a network of highly absorbing structures that we assign, for the most part, to blood vessels. In principle, some of these structures may be originated by changes in optical transmission resulting from variations in breast tissue thickness. Potential candidates are structures parallel to the breast edge that are particularly visible in the left breast of subject No. 17 [Fig. 5(a)], and are also present in other second-derivative images [Figs. 2(a), 3(b) and 4(b)]. However, these are only a minority of the visible structures, and even if their origin is indeed determined by a change in tissue thickness, the oxygenation values associated with them, being

J. Innov. Opt. Health Sci. 2010.03:267-277. Downloaded from www.worldscientific.com
by HUAZHONG UNIVERSITY OF SCIENCE AND TECHNOLOGY on 10/24/18. Re-use and distribution is strictly not permitted, except for Open Access articles.

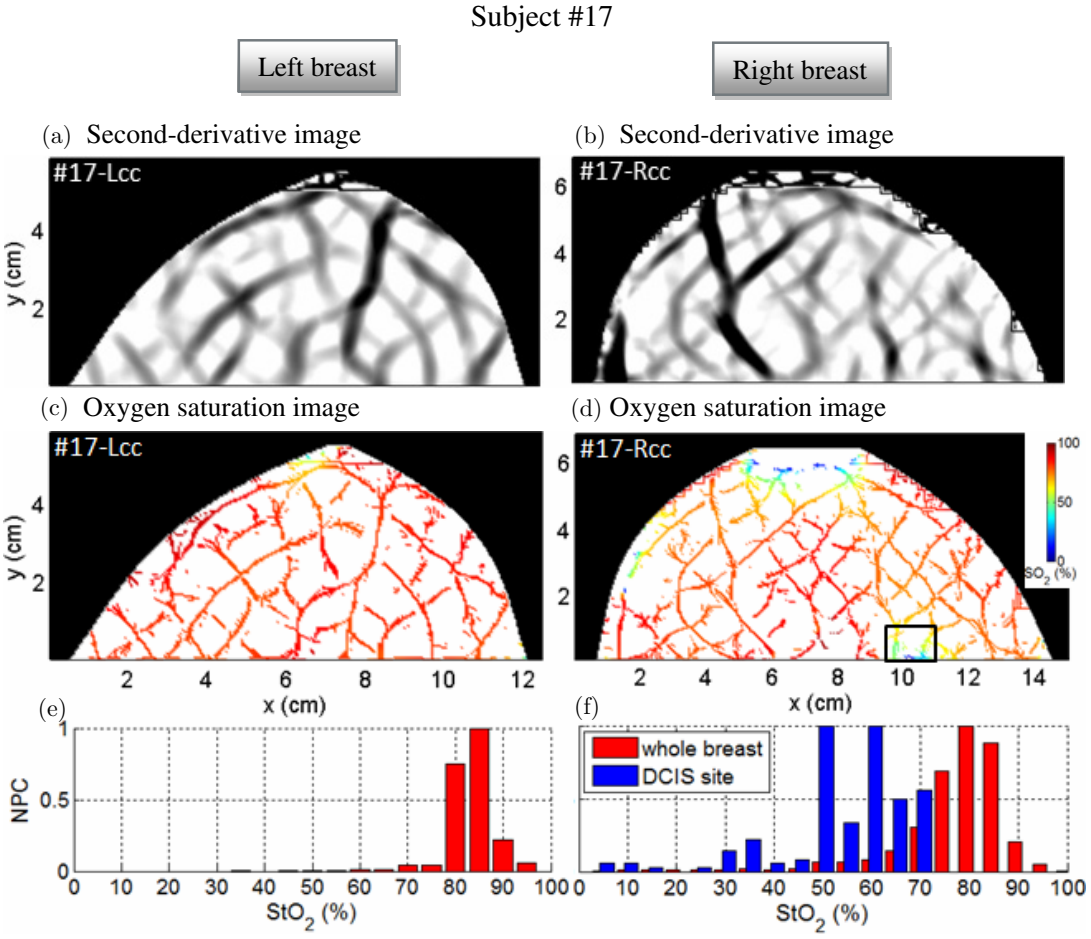

Fig. 5. Optical mammograms in a craniocaudal (cc) projection and oxygenation histograms for subject No. 17, a 56-year-old Caucasian patient with an ductal carcinoma *in situ* (DCIS) in her right breast. Panels (a) and (b) are second-derivative images, panels (c) and (d) are oxygenation images, and panels (e) and (f) are oxygenation histograms reporting the normalized pixel counts (NPC) corresponding to oxygenation values over the entire 0–100% range. Left panels [(a), (c) and (e)] refer to the left breast. Right panels [(b), (d) and (f)] refer to the right breast. The average oxygenation values in (c) and (d), as computed from the corresponding histograms in (e) and (f), are 83% for the left breast and 77% for the right breast. The histogram of the distribution of oxygenation values within the cancer region highlighted in panel (d) is shown by the blue bars in panel (f), which feature an average oxygenation of 58%.

representative of breast tissue, are still meaningful. Regarding the tissue chromophores that are at the origin of the absorbing structures displayed in the second-derivative images, they are most likely oxy-hemoglobin and deoxy-hemoglobin since they account for a blood absorption coefficient in the order of several cm^{-1}, which is much greater than the absorption coefficient of water ($\sim 10^{-2}\,cm^{-1}$)[20] or lipids ($\sim 10^{-3}\,cm^{-1}$)[21] at the wavelengths considered here.

The eight healthy subjects investigated in this work have shown comparable breast tissue oxygenation values around 85%. For the two diseased breasts of subject No. 16 and No. 17, we found statistically significant lower average oxygenation values of 61% and 77%, respectively. The local oxygenation at the cancer location was lower in the invasive ductal carcinoma (IDC) case of subject No. 16 (49%) than in the ductal carcinoma *in situ* (DCIS) case of subject No. 17 (58%). Furthermore, an area of even lower oxygenation was observed compared to the IDC site in subject No. 16. While these results were obtained from a small number of subjects (with healthy and cancer groups that were not age matched) thus awaiting validation on a larger subject pool, they nevertheless point to the potential of oxygen saturation of hemoglobin in breast tissue for the detection and discrimination of different kinds of breast cancers.

The results reported here further demonstrate the applicability of optical mammography to younger women (the average age of the

J. Innov. Opt. Health Sci. 2010.03:267-277. Downloaded from www.worldscientific.com
by HUAZHONG UNIVERSITY OF SCIENCE AND TECHNOLOGY on 10/24/18. Re-use and distribution is strictly not permitted, except for Open Access articles.

healthy subjects was 24 years) which present radiographically dense breasts, and to subjects of various ethnic groups and races (African American: subject No. 11, Caucasian: subject Nos. 12 and 17, Hispanic: subject No. 16) which feature different skin pigmentation that may in principle interfere with optical measurements.

5. Conclusion

This work represents our efforts toward developing optical mammography as a stand-alone breast imaging modality. The appeal of the method lies on the ability of optical mammography to collect breast images non-invasively and without using ionizing radiation or extrinsic contrast agents, while yielding relevant information about the spatial distribution and oxygen saturation of hemoglobin in breast tissue. Even though this work has focused on hemoglobin as the source of contrast in the optical mammograms presented, further information related to water and lipids distributions, as well as optical scattering parameters and a variety of derived optical indices are all measurable with optical mammography.[12,22,23] Our results, based on a novel spectral approach to breast tissue oximetry, point to the potential of oxygenation images in detecting breast cancer and in characterizing the metabolic state of the breast. Additional information may be provided by assessing the depth within breast tissue of the absorbing structures detected by the second-derivative images reported here. We are currently working toward this goal, to further enhance the power of optical mammography as a stand-alone diagnostic and monitoring tool.

Acknowledgment

This research was supported by the National Institutes of Health, Grant CA95885.

References

1. S. L. Jacques, B. W. Pogue, "Tutorial on diffuse light transport," *J. Biomed. Opt.* **13**, 041302 (2008).
2. D. R. Leff, O. J. Warren, L. C. Enfield, A. Gibson, T. Athanasiou, D. K. Patten, J. Hebden, G. Z. Yang, A. Darzi, "Diffuse optical imaging of the healthy and diseased breast: A systematic review," *Breast Cancer Res. Treat.* **108**, 9–22 (2008).
3. A. Hagen, D. Grosenick, R. Macdonald, H. Rinneberg, S. Burock, P. Warnick, A. Poellinger, P. M. Schlag, "Late-fluorescence mammography assesses tumor capillary permeability and differentiates malignant from benign lesions," *Opt. Express* **17**, 17016–17033 (2009).
4. S. van de Ven, A. Wiethoff, T. Nielsen, B. Brendel, M. van der Voort, R. Nachabe, M. Van der Mark, M. Van Beek, L. Bakker, L. Fels, S. Elias, P. Luijten, W. Mali, "A novel fluorescent imaging agent for diffuse optical tomography of the breast: First clinical experience in patients," *Mol. Imaging Biol.* **12**, 343–348 (2010).
5. Q. Fang, S. A. Carp, J. Selb, G. Boverman, Q. Zhang, D. B. Kopans, R. H. Moore, E. L. Miller, D. H. Brooks, D. A. Boas, "Combined optical imaging and mammography of the healthy breast: Optical contrast derived from breast structure and compression," *IEEE Trans. Med. Imaging* **28**, 30–42 (2009).
6. C. M. Carpenter, S. Srinivasan, B. W. Pogue, K. D. Paulsen, "Methodology development for three-dimensional MR-guided near infrared spectroscopy of breast tumors," *Opt. Express* **16**, 17903–17914 (2008).
7. Q. Zhu, P. U. Hegde, A. Ricci Jr, M. Kane, E. B. Cronin, Y. Ardeshirpour, C. Xu, A. Aguirre, S. H. Kurtzman, P. J. Deckers, S. H. Tannenbaum, "Early-stage invasive breast cancers: Potential role of optical tomography with US localization in assisting diagnosis," *Radiology* **256**, 367–378 (2010).
8. A. Cerussi, D. Hsiang, N. Shah, R. Mehta, A. Durkin, J. Butler, B. J. Tromberg, "Predicting response to breast cancer neoadjuvant chemotherapy using diffuse optical spectroscopy," *Proc. Natl. Acad. Sci. USA* **104**, 4014–4019 (2007).
9. S. Kukreti, A. E. Cerussi, W. Tanamai, D. Hsiang, B. J. Tromberg, E. Gratton, "Characterization of metabolic differences between benign and malignant tumors: High-spectral-resolution diffuse optical spectroscopy," *Radiology* **254**, 277–284 (2010).
10. J. Wang, S. Jiang, Z. Li, R. M. diFlorio-Alexander, R. J. Barth, P. A. Kaufman, B. W. Pogue, K. D. Paulsen, "*In vivo* quantitative imaging of normal and cancerous breast tissue using broadband diffuse optical tomography," *Med. Phys.* **37**, 3715–3724 (2010).
11. P. Taroni, A. Pifferi, E. Salvagnini, L. Spinelli, A. Torricelli, R. Cubeddu, "Seven-wavelength time-resolved optical mammography extending beyond 1000 nm for breast collagen quantification," *Opt. Express* **17**, 15932–15946 (2009).
12. R. Choe, S. D. Konecky, A. Corlu, K. Lee, T. Durduran, D. R. Busch, S. Pathak, B. J. Czerniecki, J. Tchou, D. L. Fraker, A. Demichele, B. Chance, S. R. Arridge, M. Schweiger, J. P. Culver, M. D. Schnall, M. E. Putt, M. A. Rosen, A. G. Yodh, "Differentiation of benign and malignant breast tumors by *in vivo* three-dimensional parallel-plate diffuse

optical tomography," *J. Biomed. Opt.* **14**, 024020 (2009).
13. D. R. Busch, W. Guo, R. Choe, T. Durduran, M. D. Feldman, C. Mies, M. A. Rosen, M. D. Schnall, B. J. Czerniecki, J. Tchou, A. DeMichele, M. E. Putt, A. G. Yodh, "Computer aided automatic detection of malignant lesions in diffuse optical mammography," *Med. Phys.* **37**, 1840–1849 (2010).
14. M. L. Flexman, Y. Li, A. M. Bur, C. J. Fong, J. M. Masciotti, R. Al Abdi, R. L. Barbour, A. H. Hielscher, "The design and characterization of a digital optical breast cancer imaging system," *Conf. Proc. IEEE Eng. Med. Biol. Soc.* **2008**, 3735–3738 (2008).
15. G. Boverman, Q. Fang, S. A. Carp, E. L. Miller, D. H. Brooks, J. Selb, R. H. Moore, D. B. Kopans, D. A. Boas, "Spatio-temporal imaging of the hemoglobin in the compressed breast with diffuse optical tomography," *Phys. Med. Biol.* **52**, 3619–3641 (2007).
16. N. Liu, A. Sassaroli, S. Fantini, "Paired-wavelength spectral approach to measuring the relative concentrations of two localized chromophores in turbid media: An experimental study," *J. Biomed. Opt.* **12**, 051602 (2007).
17. V. E. Pera, E. L. Heffer, H. Siebold, O. Schutz, S. Heywang-Kobrunner, L. Gotz, A. Heinig, S. Fantini, "Spatial second-derivative image processing: An application to optical mammography to enhance the detection of breast tumors," *J. Biomed. Opt.* **8**, 517–524 (2003).
18. Y. Yu, N. Liu, A. Sassaroli, S. Fantini, "Near-infrared spectral imaging of the female breast for quantitative oximetry in optical mammography," *Appl. Opt.* **48**, D225–35 (2009).
19. S. Fantini, M. A. Franceschini, G. Gaida, E. Gratton, H. Jess, W. W. Mantulin, K. T. Moesta, P. M. Schlag, M. Kaschke, "Frequency-domain optical mammography: Edge effect corrections," *Med. Phys.* **23**, 149–157 (1996).
20. G. M. Hale and M. R. Querry, "Optical constants of water in the 200-nm to 200-μm wavelength region," *Appl. Opt.* **12**, 555–563 (1973).
21. R. L. van Veen, H. J. Sterenborg, A. Pifferi, A. Torricelli, E. Chikoidze, R. Cubeddu, "Determination of visible near-IR absorption coefficients of mammalian fat using time- and spatially resolved diffuse reflectance and transmission spectroscopy," *J. Biomed. Opt.* **10**, 054004 (2005).
22. D. Hsiang, N. Shah, H. Yu, M. Y. Su, A. Cerussi, J. Butler, C. Baick, R. Mehta, O. Nalcioglu, B. Tromberg, "Coregistration of dynamic contrast enhanced MRI and broadband diffuse optical spectroscopy for characterizing breast cancer," *Technol. Cancer. Res. Treat.* **4**, 549–558 (2005).
23. Q. Zhu, S. Tannenbaum, P. Hegde, M. Kane, C. Xu, S. Kurtzman, "Noninvasive monitoring of breast cancer during neoadjuvant chemotherapy using optical tomography with ultrasound localization," *Neoplasia* **10**, 1028–1040 (2008).

J. Innov. Opt. Health Sci. 2010.03:267-277. Downloaded from www.worldscientific.com
by HUAZHONG UNIVERSITY OF SCIENCE AND TECHNOLOGY on 10/24/18. Re-use and distribution is strictly not permitted, except for Open Access articles.